






PAPER

[View Article Online](#)
[View Journal](#) | [View Issue](#)Cite this: *Dalton Trans.*, 2023, **52**, 9823

Oxidative dissolution mechanism of both undoped and Gd₂O₃-doped UO₂(s) at alkaline to hyperalkaline pH†

Sonia García-Gómez, ^a Javier Giménez, ^a Ignasi Casas, ^a Jordi Llorca ^a and Joan De Pablo ^{a,b}

The dissolution rates of unirradiated UO₂ and unirradiated UO₂ doped with Gd₂O₃ were determined as a function of pH using flow-through experiments in the presence of O₂(g) and bicarbonate. The dissolution rate of non-doped UO₂ was very low under hyperalkaline conditions (pH 12–13) whereas it increased drastically as the pH decreased to 9. The dissolution of non-doped UO₂ in the pH range of 9–13 was consistent with the oxidative dissolution mechanism already described for UO₂ dissolution in the presence of bicarbonate and oxygen. XPS analysis performed on the solid after dissolution experiments at pH 10 and 13 supported the bicarbonate effect to complex UO₂²⁺ and accelerate dissolution. Moreover, UO₂ doped with Gd₂O₃ (5 wt% and 10 wt%) showed dissolution rates as low as non-doped UO₂ under hyperalkaline conditions, which were maintained throughout the pH range studied (9–13). No substantial differences in the dissolution rates between these two doping levels were found. XPS analysis evidenced a similar surface composition both at pH 10 and 13, with U(v) being the dominant oxidation state. The low dissolution rates were assumed to be a consequence of the gadolinium capacity to retard the oxidation of U(v) to U(vi). The slight increase in dissolution rates observed in the hyperalkaline region was attributed to a shift in the oxidative dissolution mechanism, in which the presence of OH[−] promotes the formation of soluble uranyl hydroxo complexes.

Received 27th April 2023,
Accepted 21st June 2023

DOI: 10.1039/d3dt01268a

rsc.li/dalton

Introduction

Modern nuclear power plants incorporate burnable neutron absorbers in the nuclear fuel because they represent a key improvement in the commercial operation of the plant. Burnable neutron absorbers extend cycle lengths by reducing the excess reactivity of fresh UO₂ fuel at the beginning of operation.¹

Gadolinia (Gd₂O₃) is the most widely used burnable neutron absorber in both PWR and BWR fuels, due to the large neutron absorption cross-section of the main isotopes of natural gadolinium (¹⁵⁵Gd and ¹⁵⁷Gd, with 60.700 and 254.000 barns, respectively).² Their daughter nuclides formed as a result of neutron absorption present significantly lower absorption cross sections compared with parent nuclides (¹⁵⁶Gd and ¹⁵⁸Gd, with only 1.71 and 2.01 barns respectively), and therefore, they are less reactive and do not interfere in the fission chain reaction.³ Gd₂O₃ has been mixed with UO₂ in the

range of 5–10 wt% for the production of neutron-absorbing fuel (NAF) since the 1970s.⁴

Studies carried out on the consequences of the incorporation of gadolinium into the crystallographic structure of UO₂ showed an interesting trend, and the presence of gadolinium in the fuel had an important impact on the rate of oxidation of U(IV) by oxygen: the oxidation of UO₂ to U₃O₈ was found to be slower in Gd₂O₃-doped UO₂^{5,6} because of changes in the formal charge on U atoms due to the presence of Gd(III).

Park and Olander⁷ showed that when Gd(III) ions substitute for U(IV) ions in solid solutions, Gd dopant-oxygen vacancy clusters (Gd(III)-Ov) are formed in order to maintain electro-neutrality, whose presence was evidenced by Raman experiments.⁸ Since Gd(III) repels nearby double charged interstitial oxygen ions, the accommodation of excess of O^{2−} ions during UO₂ oxidation would be restricted and hence, further oxidation of the matrix may be limited.

The potential capacity of gadolinium to decrease the oxidation of U(IV) might have important consequences when considering the final disposal of the spent UO₂ fuel, because its dissolution follows an oxidative dissolution mechanism in the presence of oxygen. In this mechanism, the dissolution occurs because of the formation of U(vi) surface complexes on the solid and their subsequent dissolution through reaction with

^aDepartment of Chemical Engineering, EEBE and Barcelona Research Center in Multiscale Science and Engineering, Universitat Politècnica de Catalunya (UPC), 08019 Barcelona, Spain. E-mail: sonia.garcia.gomez@upc.edu

^bEURECAT, Centre Tecnològic de Catalunya, 08243 Manresa, Spain

†Electronic supplementary information (ESI) available. See DOI: <https://doi.org/10.1039/d3dt01268a>



bicarbonate from groundwater.^{9–11} Thus, blocking the oxidation process could imply the decrease of the dissolution of the spent nuclear fuel under the conditions expected in a high-level nuclear waste repository and, consequently, the actinides and fission products released.

Actually, electrochemical experiments carried out by Razdan and Shoesmith¹² determined that the oxidation/dissolution mechanism of Gd₂O₃-doped UO₂ is the same as that of undoped UO₂, but Gd₂O₃ was able to reduce the reactivity of the UO₂ surface. Casella *et al.*¹³ observed a decrease of the UO₂ dissolution rate in oxygen when Gd₂O₃ was added into the UO₂ matrix. The authors performed experiments with five different solids (with UO₂ doped with 0–4% Gd₂O₃) at different oxygen partial pressures and a constant pH and found that the dissolution rate decreased between 5 and 9 times compared to non-doped UO₂.

In the present work, the dissolution rates of UO₂, a common chemical analogue of the UO₂ nuclear fuel, and two different Gd₂O₃ doped UO₂ (5 wt% and 10 wt%) were determined. The study was carried out in the pH range of 9–13, in order to also consider the high pH value of groundwater in contact with concrete and cementitious materials, which are being included in concepts for the disposal of different radioactive wastes^{14–16} and no data on oxidative dissolution at high pH are available in the literature.

Materials and methods

Synthesis of Gd₂O₃–UO₂ samples

UO₂ pellets provided by Empresa Nacional del Uranio S.A. (ENUSA) were ground to a fine powder. Gd₂O₃ with a purity of 99.9% (Sigma Aldrich) and a powder diameter less than 10 µm was dried in an oven (SEL-HORN “R-8 L”, Selecta) at 500 °C for 4 h and cooled down in a vacuum desiccator.

The synthesis of Gd₂O₃–UO₂ pellets was carried out following the dry mechanical mixing method described by Baena *et al.*¹⁷ Appropriate amounts of Gd₂O₃ and UO₂ powder were mixed and blended in an agate mortar to ensure a homogeneous mixture. To improve the gadolinium distribution, powders were first mixed in a proportion of 1:1. Then, additional UO₂ powder was added to the mixture to adjust the Gd₂O₃–UO₂ ratio. In addition, to obtain pellets with low porosity, a small amount (0.2 wt%) of sintering aid Al(OH)₃ (Sigma Aldrich) was added to the mixture.¹⁸ The compaction of powders into cylindrical pellets was carried out in a uniaxial manual hydraulic press (Specac) with an applied pressure of 700 MPa. The sintering of the pellets was performed using a horizontal tube furnace ST196030 HG from Hobersal. The pellets were placed in an alumina crucible with a molybdenum cover to prevent interactions between the pellets and the crucible. The pellets were sintered at 1740 °C for 8 h under a 5 vol% H₂-Ar reducing sintering atmosphere in order to avoid the oxidation of U(IV).

After the sintering process, the pellets were ground to powder using an agate mortar and a pestle. The powder was

sieved and the particles between 50 µm and 75 µm were gathered. The specific surface area was determined by BET (Micromeritics ASAP 2020 surface area and porosity analyzer) based on adsorption/desorption isotherms of nitrogen at room temperature.

Characterization of Gd₂O₃–UO₂ samples

Sample imaging of the grain morphology on the surface of the pellets after sintering was conducted by means of a Phenom XL SEM from PhenomWorld, using an electron acceleration voltage of 15 kV. The microscope was equipped with a secondary and backscattered electron detector and an energy dispersive X-ray detector (EDX) which allowed the semi-quantitative determination of the elemental composition of a single spot and of a specific area.

X-ray diffraction (XRD) analysis was performed to determine the composition and homogeneity of the sintered pellets.¹⁹ A Bruker D8 diffractometer with Cu Kα radiation ($\lambda = 1.54056 \text{ \AA}$) was used. The voltage was 45 kV and the tube current was 35 mA. Data were collected in the 2θ range of 20°–120° with a step size of 0.02° and a dwell time of 1 s per step. The obtained XRD patterns were compared to the standard database using EVA X-ray diffraction analysis software. The identification of uranium oxide was based on PDF 00-041-1422.

XPS analysis was carried out to investigate the changes in the surface oxidation state of the powders before and after dissolution experiments. XPS spectra were recorded at a pressure below 10^{−8} mbar using a SPECS system with a Phoibos MCD-9 detector and an Al anode XR50 source operating at 150 W. The accuracy of the peak positions was ±0.2 eV.

CasaXPS software (Casa Software Ltd, UK) version 2.3.25 was used for data analysis. The spectra were fitted using 30% of the Lorentzian curve and 70% of the Gaussian curve with a Shirley background correction. Energy values were referenced to the C 1s peak located at 285 eV. The uranium oxidation state (U(IV), U(V) and U(VI)) was calculated by the deconvolution of the U4f_{7/2} and U4f_{5/2} bands, based on their characteristic binding energies and the distance among them.^{20–24} In addition, the position of the satellite peaks was considered to corroborate the fitting of the data.

Leaching solution

All the solutions were prepared using ultrapure water obtained from a Milli-Q water purification system. An Orion pH meter, model 720A, was used to determine the pH of the solution and was calibrated with standard buffer solutions from Panreac (pH 7, 9 and 13). The pH in the range of 9 to 13 was adjusted by the addition of NaOH (Sigma Aldrich) when necessary. The concentration of NaHCO₃ (Sigma Aldrich) was fixed to 5 × 10^{−3} M to simulate groundwater composition in a granitic environment and the ionic strength was kept constant at 0.1 M by using NaClO₄. The leaching solution was constantly bubbled with synthetic air (21% O₂, 79% N₂) with a purity greater than 99.99% and CO₂ < 1 ppm (supplied by Messer). Experiments were conducted at room temperature.



Experimental setup (single pass flow-through equipment)

A continuous flow-through system based on a thin solid layer reactor was used.²⁵ 0.130 g of each solid (non-doped UO_2 and UO_2 doped with 5 and 10 wt% Gd_2O_3) with the same particle size was enclosed in three parallel reactors (Swinnex filter holder 13 mm) between two $0.22\ \mu\text{m}$ pore size filters made of hydrophilic PTFE, which offered high resistance to alkaline solutions.

The leaching solution was continuously pumped through three different lines (one for each reactor) with flow rates that prevented any secondary phase formation. Samples were collected periodically at the outlet of every reactor, acidified with concentrated HNO_3 and analysed by ICP-MS (7800 from Agilent Technologies). Both uranium and gadolinium concentrations in the leachate were analysed. However, whereas the uranium concentration could be accurately measured, the gadolinium concentration was found to be below the detection limit, probably due to its low dissolution under studied conditions and the small amount present in the samples. Several flow rates between 0.05 and $0.2\ \text{mL min}^{-1}$ were tested at pH 10, where the aqueous uranium concentration measured was directly proportional to the inverse of the flow rate used. This verified that the concentrations obtained corresponded to a steady state rather than solubility equilibrium, and therefore a flow rate of $0.07\ \text{mL min}^{-1}$ was selected for subsequent experiments.

Results and discussion

Characterisation of Gd_2O_3 - UO_2 samples

The surface morphology of the UO_2 doped with Gd_2O_3 (5% and 10%) pellets after the sintering process showed well-defined grain boundaries and a low porosity microstructure (ESI†). In addition, EDX performed at different points detected U and Gd in all points of all measurements with a small variation in the gadolinium content, indicating that it was homogeneously distributed in the UO_2 matrix.

On the other hand, X-ray diffraction analysis of the samples showed a unique crystalline phase (fluorite type) and no free Gd_2O_3 . The peaks corresponding to the Gd_2O_3 -doped samples were slightly shifted towards higher angles from the UO_2 reference sample (see Fig. 1), which was attributed to the lattice contraction with increasing gadolinium concentration already observed in previous studies.^{8,19,26–29}

The results obtained by SEM-EDX and XRD showed that gadolinium was homogeneously distributed in the doped- UO_2 samples and, hence, the methodology used in this work for the synthesis of Gd_2O_3 -doped UO_2 pellets was adequate.

Furthermore, measurements of initial Gd_2O_3 -doped UO_2 (5% and 10%) pellets by means of XPS showed the presence of only U(IV) on the surface, as the U 4f XPS spectra showed the characteristics associated with U(IV).²² The peak $\text{U}4f_{7/2}$ was located at a binding energy of $379.7 \pm 0.1\ \text{eV}$ and a single satellite peak was observed at a distance of $6.7\ \text{eV}$ from $\text{U}4f_{5/2}$ (ESI†).

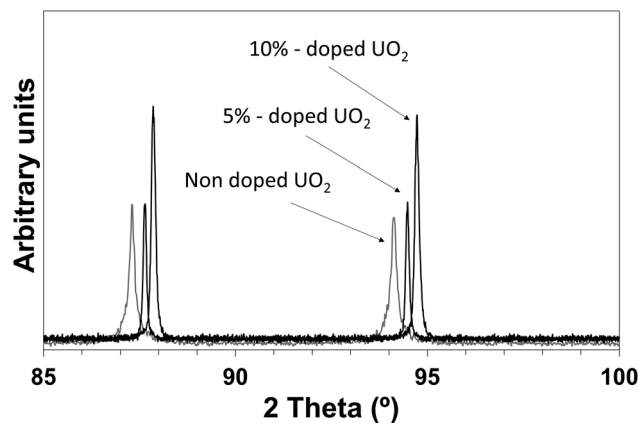


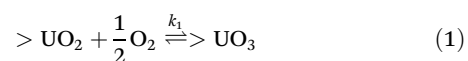
Fig. 1 Close-up of the XRD spectra of non-doped UO_2 and the solids synthesized to dope UO_2 with Gd_2O_3 . For each peak, the highest 2 theta value corresponded to 10% Gd_2O_3 doped UO_2 and the lowest to non-doped UO_2 .

Non-doped UO_2 dissolution rates

From the uranium concentrations at the steady state, the dissolution rates were calculated considering the specific surface area of the solid, measured by the BET methodology ($0.0444 \pm 0.0005\ \text{m}^2\ \text{g}^{-1}$). The non-doped UO_2 dissolution rates are presented in Table 1 and plotted in Fig. 2 as a function of pH. The main trend observed is the dependence of the dissolution rate on pH, with very low rates at pH higher than 11 and higher dissolution rates in a slightly alkaline region (between pH 9 and 10). The dissolution rates in this pH range are comparable to that reported in the literature under similar conditions using uranium dioxide⁹ and spent nuclear fuel.³⁰

De Pablo *et al.*⁹ proposed a mechanism for the dissolution of uranium dioxide in bicarbonate media and in the presence of oxygen. The oxidative dissolution mechanism consisted of three consecutive steps:

(1) Oxidation of the surface of the solid, with kinetic constants k_1 and k_{-1} .



(2) Surface coordination of U(VI) by HCO_3^- , with kinetic constant k_2 .

Table 1 Dissolution rates of UO_2 and UO_2 doped with Gd_2O_3 (5% and 10%) at different pH values

pH	$r_{\text{diss}}\text{U} \times 10^{11} (\text{mol m}^{-2} \text{s}^{-1})$		
	0% Gd_2O_3	5% Gd_2O_3	10% Gd_2O_3
9	28.95 ± 0.50	1.77 ± 0.50	1.38 ± 0.50
10	26.37 ± 0.50	0.91 ± 0.50	0.84 ± 0.50
11	15.18 ± 0.50	0.45 ± 0.50	0.65 ± 0.50
11.5	4.86 ± 0.50	0.24 ± 0.50	0.37 ± 0.50
12	0.57 ± 0.50	0.32 ± 0.50	0.32 ± 0.50
12.5	0.51 ± 0.50	0.37 ± 0.50	0.47 ± 0.50
13	0.49 ± 0.50	0.54 ± 0.50	0.60 ± 0.50



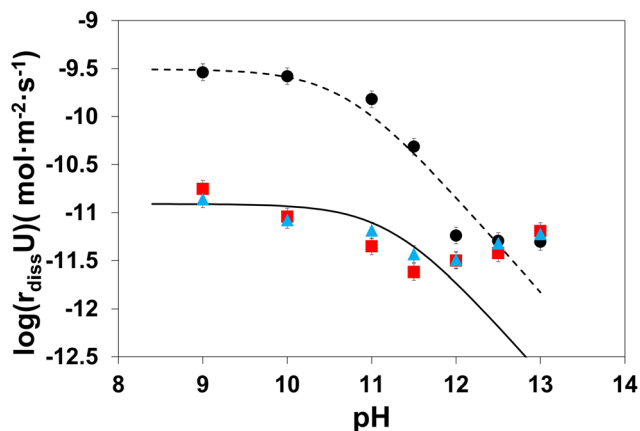
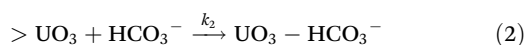
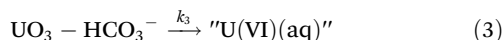


Fig. 2 UO_2 and Gd_2O_3 -doped UO_2 dissolution rates determined in this work as a function of pH (● non-doped UO_2 , ■ 5% Gd_2O_3 doped UO_2 ; ▲ 10% Gd_2O_3 doped UO_2) and fitting of the oxidative dissolution model from eqn (4) using the parameters from Table 2 (dashed and straight lines for modelling non-doped and doped UO_2 dissolution rates, respectively).



(3) Dissolution of the U(VI) -bicarbonate species formed on the surface, with kinetic constant k_3 . This step was considered very fast, and consequently, the dissolution rate depends only on k_1 , k_{-1} and k_2 constants.



Considering this mechanism, the dissolution rate could be calculated using eqn (4) as a function of oxygen and bicarbonate concentrations in solution as well as the number of U(IV) sites in the solid surface, $\{>\text{UO}_2\}_{\text{tot}}$, with a value of $10^{-6} \text{ mol m}^{-2}$.³¹ Details of how to determine eqn (4) from this mechanism are provided by De Pablo *et al.*⁹

$$r_{\text{diss}} \text{U} (\text{mol m}^{-2} \text{s}^{-1}) = \frac{k_1 k_2 \{>\text{UO}_2\}_{\text{tot}} [\text{O}_2] [\text{HCO}_3^-]}{k_{-1} + k_2 [\text{HCO}_3^-] + k_1 [\text{O}_2]} \quad (4)$$

In this work, where the pH of the solution is varied, it is necessary to consider that the free bicarbonate concentration in solution depends on pH. Considering the equations of the total carbon concentration in the alkaline region (eqn (5)),

$$\text{Total}_{\text{conc.}} = [\text{HCO}_3^-] + [\text{CO}_3^{2-}] \quad (5)$$

and the equilibrium constant between carbonate and bicarbonate (eqn (6)).

$$K_2 = \frac{[\text{CO}_3^{2-}][\text{H}^+]}{[\text{HCO}_3^-]} \quad (6)$$

The free bicarbonate concentration in eqn (4) should be substituted by the expression in eqn (7).

$$[\text{HCO}_3^-] = \frac{\text{Total}_{\text{conc.}}}{\frac{K_2}{[\text{H}^+]} + 1} \quad (7)$$

Fig. 2 shows the fitting of the oxidative dissolution model to the dissolution rates determined in this work. The kinetic

constant values are presented in Table 2, with the k_2 constant being a bit higher than that obtained by de Pablo *et al.*⁹ at 25 °C. The good fitting of the model to the experimental data indicates that the UO_2 oxidative dissolution model is able to reproduce the behaviour of the dissolution rates in a wide pH range. In addition, the decrease of the dissolution rate at relatively high pH values is a consequence of the absence of bicarbonate due to acid–base reactions.

At such pH values, uranium is oxidized to U(VI) through the first step of the oxidative dissolution mechanism, and the determinant step would be the formation of surface complexes between U(VI) and bicarbonate (step 2 of the mechanism). The results would confirm that carbonate (predominant species in this pH range) is not able to substitute bicarbonate in the detachment of U(VI) from the solid to the solution, as was previously suggested.^{9,32} The critical dependence of the dissolution rate with free bicarbonate in solution can be seen in Fig. 3, which shows that the main parameter that affects the UO_2 dissolution rate in oxygen is the free bicarbonate in solution.

The solid surface of UO_2 samples was analysed by XPS after dissolution experiments at pH 10 and 13. Fig. 4(a) and (b) show the deconvoluted spectra for the $\text{U } 4f_{7/2}$ and $\text{U } 4f_{5/2}$ peaks and their corresponding satellites. The percentages of U(IV) , U(V) and U(VI) are presented in Table 3. These results indicate

Table 2 Results of fitting eqn (4) to the experimental data

Sample	k_1	k_{-1}	k_2
UO_2	2.0 ± 0.1	$(1.0 \pm 0.4) \times 10^{-4}$	0.15 ± 0.02
UO_2 -5% Gd_2O_3	0.05 ± 0.01	$(1.0 \pm 0.4) \times 10^{-4}$	0.15 ± 0.02
UO_2 -10% Gd_2O_3	0.05 ± 0.01	$(1.0 \pm 0.4) \times 10^{-4}$	0.15 ± 0.02

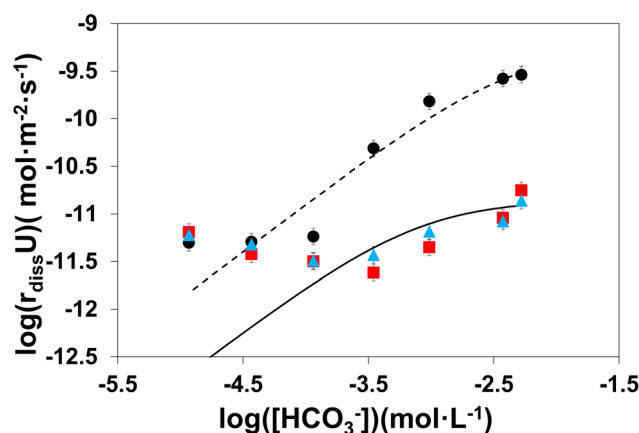


Fig. 3 UO_2 and Gd_2O_3 -doped UO_2 dissolution rates determined in this work as a function of the bicarbonate concentration (● non-doped UO_2 , ■ 5% Gd_2O_3 doped UO_2 ; ▲ 10% Gd_2O_3 doped UO_2) and fitting of the oxidative dissolution model from eqn (4) using the parameters from Table 2, considering the variation of the free bicarbonate ion in solution (dashed and straight lines for modelling non-doped and doped UO_2 dissolution rates, respectively).



that the higher the bicarbonate concentration in solution, the lower the $U(VI)$ amount on the surface. This finding correlates dissolution with $U(VI)$ on the surface, which is consistent with the ability of HCO_3^- to coordinate $U(VI)$ species.^{33–36}

Gd₂O₃-doped UO₂ dissolution rates

The oxidative dissolution of Gd₂O₃-UO₂ powders was compared to UO₂ powder under the same experimental conditions. Fig. 2 shows the dissolution rates of the doped samples as a function of pH together with the non-doped UO₂ dissolution rates. The main trend observed is that the doping of gadolinium oxide showed a drastic decrease of the UO₂ dissolution rate in the alkaline pH range. The dissolution rates of the gadolinium-doped solids at pH 9 are as low as 2×10^{-11} mol m⁻² s⁻¹, more than 15 times lower than that of non-doped UO₂ at the same pH. The obtained low dissolution rates make

Table 3 XPS results after dissolution experiments: FWHM and binding energy values of the U4f_{7/2} peak and the percentage of U(IV), U(V) and U(VI) on the surface of the sample

Sample	pH	FWHM U4f _{7/2} (eV)	BE U4f _{7/2} (eV)	%U		
				U(IV)	U(V)	U(VI)
UO ₂	10	2.6 ± 0.2	380.3 ± 0.2	47 ± 5	49 ± 5	4 ± 5
UO ₂	13	3.0 ± 0.2	380.7 ± 0.2	27 ± 5	53 ± 5	20 ± 5
UO ₂ -10% Gd ₂ O ₃	10	2.5 ± 0.2	380.5 ± 0.2	19 ± 5	72 ± 5	9 ± 5
UO ₂ -10% Gd ₂ O ₃	13	2.5 ± 0.2	380.5 ± 0.2	25 ± 5	67 ± 5	8 ± 5

it difficult to ascertain if there is a dependency with the gadolinium content of the solid, although it seems that similar rates were obtained with both doped solids, and the main effect of the presence of gadolinium on the dissolution rates would be already at the solid doped with 5% Gd₂O₃. A decrease of the

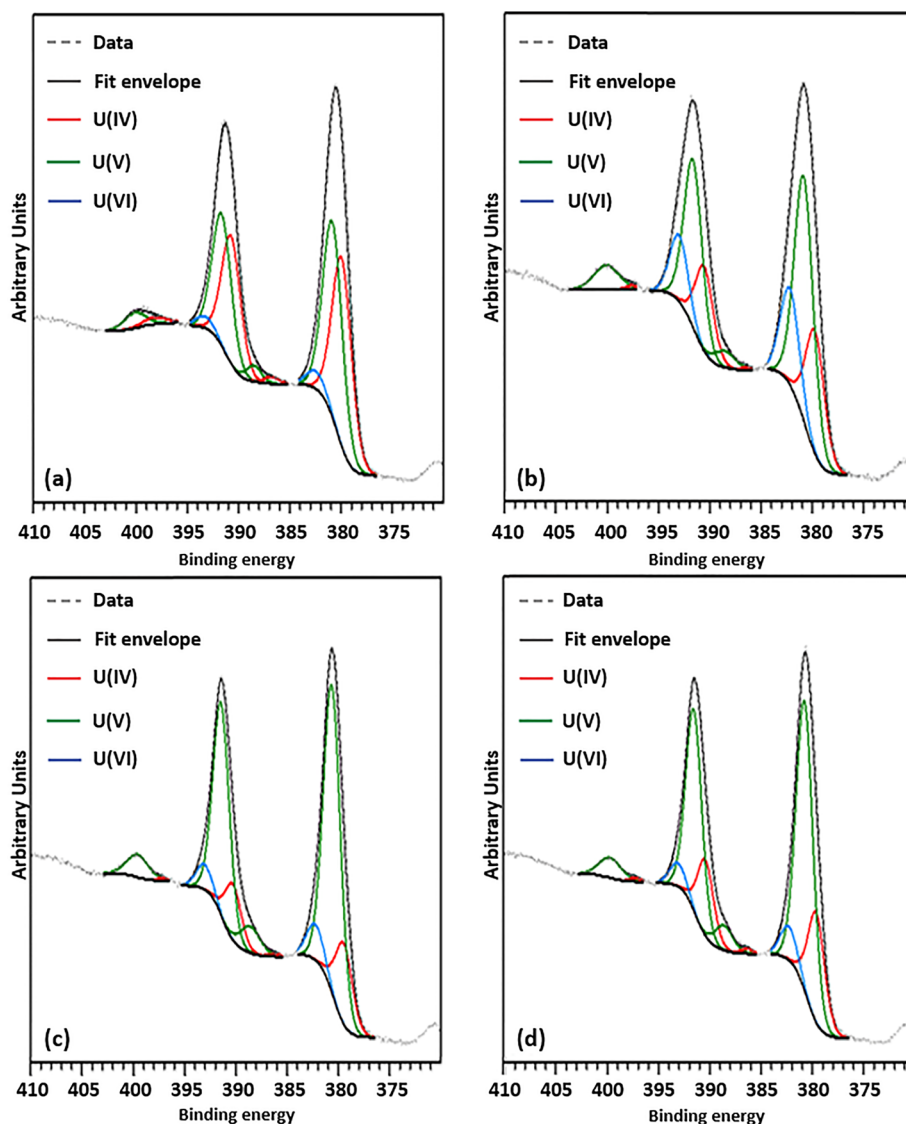


Fig. 4 U4f XPS spectra resolved into U(IV), U(V) and U(VI) contributions recorded after dissolution experiments on (a) UO₂ at pH 10, (b) UO₂ at pH 13, (c) UO₂-10% Gd₂O₃ at pH 10 and (d) UO₂-10% Gd₂O₃ at pH 13.



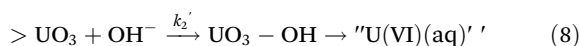
Table 4 Limiting steps of the oxidative dissolution mechanism considering the pH of the dissolution and the type of solid

pH	Type of solid	Oxidation step	Dissolution step
10	Non-doped UO ₂	Not limited: >U(IV) → >U(V) → >U(VI)	Not limited: >U(VI) + HCO ₃ → U(VI)(aq)
10	Gd ₂ O ₃ -doped UO ₂	Limited: >U(IV) → >U(V)	
13	Non-doped UO ₂	Not limited: >U(IV) → >U(V) → >U(VI)	Limited: >U(VI)
13	Gd ₂ O ₃ -doped UO ₂	Limited: >U(IV) → >U(V)	

dissolution rate with the gadolinium content (0–4% Gd₂O₃ doped UO₂ solids) at different oxygen concentrations at pH close to 8 in the presence of bicarbonate was already detected by Casella *et al.*¹³ The authors determined an 8-times decrease of the dissolution rate of 4% Gd₂O₃ at the same oxygen concentration as in this work.

The model described in eqn (4) was applied to doped samples, as can be seen in Fig. 3, where the dissolution rate was plotted against the bicarbonate concentration. The best fitting was obtained with a k_1 (the kinetic constant of the oxidation step) forty times lower than the one obtained with non-doped samples (see Table 2), indicating a slower oxidation rate. Therefore, the decrease in the amount of uranium released in the doped solids at alkaline pH would be related to the influence of gadolinium on the oxidation of U(IV) to U(V) or U(VI).

However, the deviation from the model at very low bicarbonate concentrations (high pH values) could be due to the effect of OH[−] ions and the change in the oxidative dissolution mechanism. Under these conditions, a new mechanism can be described considering the surface coordination of U(VI) by OH[−], with kinetic constant k_2' , followed by a detachment of the surface complex, according to reaction (8).



where U(VI)(aq) refers to uranyl hydroxo complexes, such as UO₂(OH)₄^{2−}. Considering this step, the dissolution rate is proportional to [OH[−]] ($r_{\text{diss}} \propto k_2' [\text{OH}^-]$). This could explain the slight increase of the dissolution rate observed in the hyperalkaline region when pH increases.

XPS analysis performed on doped samples after dissolution experiments at pH = 10 and pH = 13 (Fig. 4(c) and (d)) showed similar uranium oxidation state compositions (see Table 3). From the relatively high U(V) percentage of the two doped UO₂ solids, it is possible to establish the oxidative dissolution mechanism, as well as the limiting step, as a function of pH and the type of solid (see Table 4).

- At pH 10: The dissolution rates of non-doped UO₂ are relatively high since U(IV) is being oxidized to U(VI) by oxygen and the U(VI) formed on the surface is being dissolved as there is enough bicarbonate in solution. However, for Gd₂O₃-doped UO₂, the presence of gadolinia retards the oxidation step; U(IV) is not fully oxidized to U(VI), but to U(V), according to the XPS data (Fig. 4), and the dissolution rates are much smaller in spite of the presence of bicarbonate.

- At pH 13: The low dissolution rates determined for non-doped UO₂ (compared to pH = 10) are due to the low bicarbon-

ate concentration in solution; U(IV) is being oxidized to U(VI) but less dissolved by OH[−]. On the other hand, for Gd₂O₃-doped UO₂, the dissolution process is limited by the oxidation of the surface, U(IV) oxidizes mainly to U(V) but not to U(VI).

As can be seen, the main influence of gadolinia would be the retardation of UO₂ oxidation by oxygen, with a relatively high U(IV) → U(V) conversion, which would not go further. This is consistent with the findings of Scheele *et al.*⁶ and Razdan *et al.*,¹² who reported that Gd doping leads to the stability of the U₃O₇/U₄O₉ cubic oxidation product and inhibits or delays its further oxidation to U₃O₈.

Considering the increasing use of gadolinia as a burnable neutron absorber in modern nuclear plants, its impact on the final disposal of the spent nuclear fuel is of great importance and should be investigated. From this point of view, doping with gadolinium oxide points to a positive impact on the release of uranium and other radionuclides to the biosphere after the contact between the fuel and groundwater in a wide pH range. The retardation of UO₂ matrix dissolution would not only decrease the release of uranium to the near field of the repository, but also the release of radionuclides contained in the fuel matrix. As observed in Fig. 3, the “passivation” of UO₂ would occur in the whole pH range expected for groundwater that might come in contact with the nuclear fuel, from bicarbonated water (pH 8–9) to water that was in contact with cementitious materials used in the high-level nuclear waste repository (pH 12–13.5).

Conclusions

In experiments where the formation of secondary solid phases is avoided, UO₂ dissolution rates determined at alkaline to hyperalkaline pH agree with the oxidative dissolution mechanism described by de Pablo *et al.*⁹ At pH > 10, the dissolution rates were very low compared to alkaline pH, due to the predominance of the carbonate ion instead of the bicarbonate ion. XPS results evidenced that in the presence of bicarbonate (pH 10), the U(VI) amount on the surface was very low, denoting that the UO₂²⁺ species were dissolved in solution, while at pH 13 and in the absence of bicarbonate, the amount of U(VI) observed was higher.

The doping of UO₂ with gadolinium oxide resulted in relatively low dissolution rates. In particular, at pH < 10, dissolution rates of Gd₂O₃-doped UO₂ were about 15 times lower than those of non-doped UO₂. The lower dissolution rates could be due to the capacity of gadolinium to prevent uranium



oxidation. Gd₂O₃-doped UO₂ dissolution rates were fitted with the same model used previously with UO₂. In this case, the best fitting was obtained with the k_1 parameter forty times lower than with undoped UO₂, showing retardation of the oxidation rate. The slight increase in dissolution rates observed at high pH was attributed to a change in the oxidative dissolution mechanism, where soluble uranyl hydroxo complexes may be formed due to the effect of OH[−] ions. XPS analysis performed both at pH 10 and 13 pointed out that U(v) was the dominant oxidation state present on the surface, which may indicate that gadolinia enhances the stability of U(v), delaying the subsequent oxidation to U(vi). A similar surface composition obtained in both experiments was in agreement with the dissolution rates observed.

The decrease of UO₂ dissolution in the doped solids would have a positive impact on the release of uranium and other radionuclides to the groundwater expected to be in contact with the spent nuclear fuel.

Author contributions

Conceptualization, I. C. and J. P.; methodology, I. C.; data collection, J. L.; investigation and writing – original draft, S. G.-G.; supervision and writing – review & editing, J. G., I. C., J. L. and J. P.; funding acquisition, J. P.; all authors have read and agreed to the published version of the manuscript.

Conflicts of interest

There are no conflicts to declare.

Acknowledgements

This work has been financially supported by Ministerio de Economía y Competitividad (Spain) with the projects PID2020-116839RB-I00 and ENE2017-83048-R. ENRESA is also acknowledged for its interest and financial support (Project 079-CO-IA-2020-0001 and CO-IA-22-010). S. García-Gómez wants to acknowledge the fellowship with reference code PRE2018-085618. J. Llorca is a Serra Hùnter Fellow and is grateful to the ICREA Academia program. We are thankful to Centres científics i tecnològics: Unitat d'anàlisi de superfícies (CCiTUB) for some XPS measurements. We acknowledge the constructive comments of the reviewers to help us improve the quality of the article.

References

- 1 L. Frybortova, VVER-1000 fuel cycles analysis with different burnable absorbers, *Nucl. Eng. Des.*, 2019, **351**, 167–174.
- 2 G. Leinweber, D. P. Barry, M. J. Trbovich, J. A. Burke, N. J. Drindak, H. D. Knox, R. V. Ballard, R. C. Block, Y. Danon and L. I. Severnyak, Neutron capture and total cross-section measurements and resonance parameters of gadolinium, *Nucl. Sci. Eng.*, 2006, **154**, 261–279.
- 3 IAEA, *Characteristics and Use of Urania-Gadolinia Fuels*, TecDoc-844, 1995.
- 4 IAEA, *Experiences and trends of manufacturing technology of advanced nuclear fuel*, TecDoc-1686, 2012.
- 5 J. G. Kim, Y. K. Ha, S. D. Park, K. Y. Jee and W. H. Kim, Effect of a trivalent dopant, Gd³⁺, on the oxidation of uranium dioxide, *J. Nucl. Mater.*, 2001, **297**, 327–331.
- 6 R. D. Scheele, B. D. Hanson and A. M. Casella, Effect of added gadolinium oxide on the thermal air oxidation of uranium dioxide, *J. Nucl. Mater.*, 2021, **552**, 153008.
- 7 K. Park and D. R. Olander, Defect models for the oxygen potentials of gadolinium-and europium-doped urania, *J. Nucl. Mater.*, 1992, **187**, 89–96.
- 8 J. Lee, J. Y. G. J. Kim, Y. S. Youn, N. Liu, J. Y. G. J. Kim, Y. K. Ha, D. W. Shoesmith and J. Y. G. J. Kim, Raman study on structure of U_{1-y}Gd_yO_{2-x} (y=0.005, 0.01, 0.03, 0.05 and 0.1) solid solutions, *J. Nucl. Mater.*, 2017, **486**, 216–221.
- 9 J. de Pablo, I. Casas, J. Giménez, M. Molera, M. Rovira, L. Duro and J. Bruno, The oxidative dissolution mechanism of uranium dioxide. I. The effect of temperature in hydrogen carbonate medium, *Geochim. Cosmochim. Acta*, 1999, **63**, 3097–3103.
- 10 J. Giménez, F. Clarens, I. Casas, M. Rovira, J. De Pablo and J. Bruno, Oxidation and dissolution of UO₂ in bicarbonate media: Implications for the spent nuclear fuel oxidative dissolution mechanism, *J. Nucl. Mater.*, 2005, **345**, 232–238.
- 11 J. Merino, E. Cera, J. Bruno, J. Quiñones, I. Casas, F. Clarens, J. Giménez, J. De Pablo, M. Rovira and A. Martínez-Esparza, Radiolytic modelling of spent fuel oxidative dissolution mechanism. Calibration against UO₂ dynamic leaching experiments, *J. Nucl. Mater.*, 2005, **346**, 40–47.
- 12 M. Razdan and D. W. Shoesmith, The Electrochemical Reactivity of 6.0 wt% Gd-Doped UO₂ in Aqueous Carbonate/Bicarbonate Solutions, *J. Electrochem. Soc.*, 2014, **161**, H225–H234.
- 13 A. Casella, B. Hanson and W. Miller, The effect of fuel chemistry on UO₂ dissolution, *J. Nucl. Mater.*, 2016, **476**, 45–55.
- 14 F. J. Huertas, A. Hidalgo, M. L. Rozalén, S. Pellicione, C. Domingo, C. A. García-González, C. Andrade and C. Alonso, Interaction of bentonite with supercritically carbonated concrete, *Appl. Clay Sci.*, 2009, **42**, 488–496.
- 15 I. Rojo, M. Rovira and J. de Pablo, Selenate Diffusion Through Mortar and Concrete, *Environ. Eng. Sci.*, 2014, **31**, 469–473.
- 16 T. Heath, J. Schofield and A. Shelton, Understanding cementitious backfill interactions with groundwater components, *Appl. Geochemistry*, 2020, **113**, 104495.
- 17 A. Baena, T. Cardinaels, B. Vos, K. Binnemans and M. Verwerft, Synthesis of UO₂ and ThO₂ doped with Gd₂O₃, *J. Nucl. Mater.*, 2015, **461**, 271–281.
- 18 L. R. dos Santos, M. Durazzo, E. F. Urano de Carvalho and H. G. Riella, Effect of Al(OH)₃ on the sintering of UO₂–Gd₂O₃ fuel pellets with addition of U₃O₈ from recycle, *J. Nucl. Mater.*, 2017, **493**, 30–39.



- 19 A. G. Leyva, D. Vega, V. Trimarco and D. Marchi, Homogeneity characterisation of sintered (U,Gd)O₂ pellets by X-ray diffraction, *J. Nucl. Mater.*, 2002, **303**, 29–33.
- 20 E. S. Ilton, J. F. Boily and P. S. Bagus, Beam induced reduction of U(VI) during X-ray photoelectron spectroscopy: The utility of the U4f satellite structure for identifying uranium oxidation states in mixed valence uranium oxides, *Surf. Sci.*, 2007, **601**, 908–916.
- 21 M. Schindler, F. C. Hawthorne, M. S. Freund and P. C. Burns, XPS spectra of uranyl minerals and synthetic uranyl compounds. I: The U 4f spectrum, *Geochim. Cosmochim. Acta*, 2009, **73**, 2471–2487.
- 22 Y. A. Teterin, A. J. Popel, K. I. Maslakov, A. Y. Teterin, K. E. Ivanov, S. N. Kalmykov, R. Springell, T. B. Scott and I. Farnan, XPS Study of Ion Irradiated and Unirradiated UO₂ Thin Films, *Inorg. Chem.*, 2016, **55**, 8059–8070.
- 23 E. S. Ilton and P. S. Bagus, XPS determination of uranium oxidation states, *Surf. Interface Anal.*, 2011, **43**, 1549–1560.
- 24 J. F. Boily and E. S. Ilton, An independent confirmation of the correlation of U4f primary peaks and satellite structures of U^{VI}, U^V and U^{IV} in mixed valence uranium oxides by two-dimensional correlation spectroscopy, *Surf. Sci.*, 2008, **602**, 3637–3646.
- 25 J. Bruno, I. Casas and I. Puigdomènech, The kinetics of dissolution of UO₂ under reducing conditions and the influence of an oxidized surface layer (UO_{2+x}): Application of a continuous flow-through reactor, *Geochim. Cosmochim. Acta*, 1991, **55**, 647–658.
- 26 M. Durazzo and H. G. Riella, Studies on the Sintering Behaviour of UO₂-Gd₂O₃ Nuclear Fuel, *Int. Youth Nucl. Congr.*, 2008, 20–26.
- 27 S. Fukushima, T. Ohmichi, A. Maeda and H. Watanabe, The effect of gadolinium content on the thermal conductivity of near-stoichiometric (U,Gd)O₂ solid solutions, *J. Nucl. Mater.*, 1982, **105**, 201–210.
- 28 A. Baena, T. Cardinaels, K. Govers, J. Pakarinen, K. Binnemans and M. Verwerft, Lattice contraction and lattice deformation of UO₂ and ThO₂ doped with Gd₂O₃, *J. Nucl. Mater.*, 2015, **467**, 135–143.
- 29 K. Kapoor, S. V. Ramana Rao, Sheela, T. Sanyal and A. Singh, Study on solid solubility of Gd in UO₂ using X-ray diffraction, *J. Nucl. Mater.*, 2003, **321**, 331–334.
- 30 W. J. Gray, H. R. Leider and S. A. Steward, Parametric study of LWR spent fuel dissolution kinetics, *J. Nucl. Mater.*, 1992, **190**, 46–52.
- 31 J. A. Davis and D. B. Kent, Surface Complexation Modeling in Aqueous Geochemistry, ed. M. F. Hochella and A. F. White, in *Mineral-Water Interface Geochemistry*, Min. Soc. Am. Rev. Mineral., 1990, vol. 23, pp. 177–260.
- 32 G. F. Thomas and G. Till, The dissolution of unirradiated UO₂ fuel pellets under simulated disposal conditions, *Nucl. Chem. Waste Manage.*, 1984, **5**, 141–147.
- 33 J. Bruno, I. Casas, E. Cera, J. De Pablo, J. Giménez and M. E. Torrero, Uranium(IV) dioxide and simfuel as chemical analogues of nuclear spent fuel matrix dissolution. A comparison of dissolution results in a standard NaCl/NaHCO₃ solution, *Mat. Res. Soc. Symp. Proc.*, 1995, **353**, 601–608.
- 34 J. De Pablo, I. Casas, J. Giménez, V. Martí and M. E. Torrero, Solid surface evolution model to predict uranium release from unirradiated UO₂ and nuclear spent fuel dissolution under oxidizing conditions, *J. Nucl. Mater.*, 1996, **232**, 138–145.
- 35 J. S. Goldik, J. J. Noël and D. W. Shoesmith, Surface electrochemistry of UO₂ in dilute alkaline hydrogen peroxide solutions: Part II. Effects of carbonate ions, *Electrochim. Acta*, 2006, **51**, 3278–3286.
- 36 M. M. Hossain, E. Ekeröth and M. Jonsson, Effects of HCO₃[−] on the kinetics of UO₂ oxidation by H₂O₂, *J. Nucl. Mater.*, 2006, **358**, 202–208.

